



Cite this: *CrystEngComm*, 2021, 23, 1294

## Pre-organisation of ligand donor sets modulates the supramolecular structure of bis(pyridyl–imine) silver(I) chelates†

Chané Venter and Matthew P. Akerman \*

Three bis(pyridyl–imine) ligands 1,2-bis(2-pyridyliminomethyl)benzene (**L1**), 1,3-bis(2-pyridyliminomethyl)benzene (**L2**) and 1,4-bis(2-pyridyliminomethyl)benzene (**L3**) were synthesised and complexed to silver(I) salts forming four novel complexes; 1,2-bis(2-pyridyliminomethyl)benzene–silver(I) hexafluoroantimonate(V) [Ag(**L1**)](SbF<sub>6</sub>), bis(1,3-bis(2-pyridyliminomethyl)benzene–di–silver(I) bis(hexafluoroantimonate(V)) [Ag<sub>2</sub>–μ–(**L2**)<sub>2</sub>](SbF<sub>6</sub>)<sub>2</sub>, *catena*-1,4-bis(2-pyridyliminomethyl)benzene–silver(I) hexafluoroantimonate(V) [Ag–μ–(**L3**)](SbF<sub>6</sub>) and *catena*-1,4-bis(2-pyridyliminomethyl)benzene–silver(I) tetraphenylborate(III) [Ag–μ–(**L3**)](BPh<sub>4</sub>). All four complexes were characterized by <sup>1</sup>H and <sup>13</sup>C NMR, IR, mass spectrometry and UV/visible spectroscopy as well as X-ray crystallography. The ligands were designed to preorganise the atom donor sets to control the structures of the metal chelates. The pre-organised ligands control the supramolecular structure of the bis(pyridyl–imine) silver(I) chelates, which results in the formation of a monomeric structure for chelate [Ag(**L1**)](SbF<sub>6</sub>), a dimeric structure for chelate [Ag<sub>2</sub>–μ–(**L2**)<sub>2</sub>](SbF<sub>6</sub>)<sub>2</sub>, and polymeric structures for chelates [Ag–μ–(**L3**)](SbF<sub>6</sub>) and [Ag–μ–(**L3**)](BPh<sub>4</sub>). The d<sup>10</sup> electronic configuration of silver allows the metal ion to adopt both tetrahedral and square planar coordination geometries in the above compounds, assisting the formation of the various compounds. Additionally, the stabilising effects of the intermolecular interactions were studied using DFT methods.

Received 6th November 2020,  
Accepted 8th January 2021

DOI: 10.1039/d0ce01610a

[rsc.li/crystengcomm](http://rsc.li/crystengcomm)

## Introduction

Crystal engineering and the design of porous materials for small molecule storage has been an area of intense research in recent years. To this end, understanding the influence ligand donor set geometry has on the supramolecular structure of coordination compounds is highly relevant.<sup>1–4</sup> Schiff base ligands are commonly used to stabilise metal ions in various oxidation states through coordination.<sup>2,5</sup> Their application spans a range of fields including: catalysis, metallodrugs, metal extraction and, significantly, crystal engineering.<sup>2,5,6–9</sup> The coordination of silver(I) to neutral, tetradentate N-donor Schiff base ligands is relatively uncommon; with metals ions such as Cu(II), Zn(II), Mn(II), Co(II), Ni(II), and Au(III), among others, being more frequently coordinated to these Schiff base ligands.<sup>8–16</sup>

The study of silver(I) coordination complexes with rigid or flexible bis(pyridyl) ligands is gaining interest in the fields of

crystal engineering and coordination chemistry.<sup>17–20</sup> A study done by Deng *et al.* illustrates silver(I) being coordinated to flexible bis(pyridyl–amine) ligands with various spacers, forming bimetallic structures.<sup>19</sup> Since silver(I) has a d<sup>10</sup> electronic configuration and hence zero crystal field stabilisation energy (CFSE), a range of coordination geometries are possible. This makes it a suitable candidate for testing the impact of ligand geometry on the resultant structure of supramolecular compounds. The range of coordination geometries that are possible with little or no energy cost has led to some interesting compounds such as helical silver(I) coordination polymers from flexible bis(pyridyl) ligands.<sup>17</sup> The flexible coordination geometry of silver(I) is potentially ideal for crystal engineering as small changes in the structures of ligands and/or counter ions can lead to noticeable changes in the three-dimensional crystal lattice.

The various regioisomers of the bis(pyridyl–imine) ligands with rigid aromatic di(azomethine) linkages have found widespread application. 1,2-Bis(2-pyridyliminomethyl)benzene has been used to stabilise trivalent lanthanide metals for applications as biological markers, photodynamic therapeutics, NMR contrast reagents and phosphoryl transfer catalysts.<sup>21</sup> This regioisomer of the ligand has also been coordinated to Ni(II), Cu(II) and Fe(II) which led to mononuclear complexes in all cases.<sup>22,23</sup> The ligand 1,4-bis(2-

School of Chemistry and Physics, University of KwaZulu-Natal, Private Bag X01, Scottsville, Pietermaritzburg, 3209, South Africa. E-mail: akermanm@ukzn.ac.za  
 † Electronic supplementary information (ESI) available. CCDC 2033490–2033493, contains the crystallographic data for compounds [Ag(**L1**)](SbF<sub>6</sub>), [Ag<sub>2</sub>–μ–(**L2**)<sub>2</sub>](SbF<sub>6</sub>)<sub>2</sub>, [Ag–μ–(**L3**)](SbF<sub>6</sub>) and [Ag–μ–(**L3**)](BPh<sub>4</sub>), respectively. For ESI and crystallographic data in CIF or other electronic format see DOI: 10.1039/d0ce01610a

pyridyliminomethyl)benzene has been complexed to Re(III) and Ir(III) and the crystallographic and luminescent properties of the complexes studied.<sup>24,25</sup> A series of phenylene-bridged dimer species complexed to Re(III) have been synthesised and studied crystallographically. The dimeric *meta*- and *para*-phenylenediamine-bridged metal compounds were investigated for photophysical applications using UV-visible spectroscopy and cyclic voltammetry.<sup>26</sup> Similar ligands *ortho*-, *meta*- and *para*-bis(imino-pyrrole) benzene forming three semi-rigid isomeric molecules have also been studied. These examples show the significance of pre-organisation of atom donor sets of free ligands for control of the supramolecular structure in nanomaterials.<sup>27</sup> The ligands are also highly conjugated  $\pi$ -systems, capable of forming myriad non-covalent interactions such as  $\pi\cdots\pi$  and  $\text{Ag}\cdots\pi$  interactions, which have been previously shown to be significant in the field of crystal engineering.<sup>28–33</sup>

Herein, we report the synthesis, solid-state structures and UV/visible spectra of four silver(I) chelates (Scheme 1). The chelates differ by the structure of the phenylenediamine bridging unit. Through pre-organisation of the ligand donor sets it is possible to control the supramolecular structure of the metal chelates. The stabilising effects of some of the intermolecular interactions are studied using DFT methods.

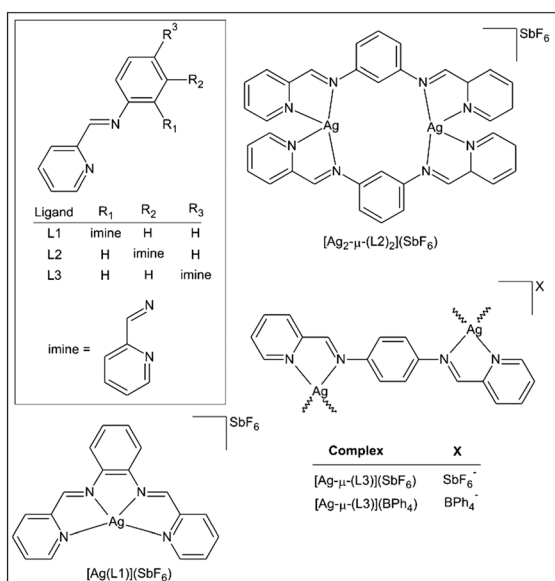
## Experimental

### Materials and methods

All reactions were carried out under inert conditions using a double manifold vacuum line, cannula techniques and Schlenkware. All reagents used in the syntheses were purchased from Sigma-Aldrich and used as received. Organic solvents were of analytical reagent grade and purchased from Merck (South Africa). All solvents were dried prior to use,

using a Puresolv™ MD 7 purification system from Innovative Technologies. NMR spectra were recorded with a Bruker Avance III 400 spectrometer equipped with a Bruker magnet (9.395 T) using a 5 mm TBIZ probe at the following frequencies:  $^1\text{H}$  = 400 MHz and  $^{13}\text{C}$  = 100 MHz. The spectra were recorded at 30 °C. All proton and carbon chemical shifts are expressed in parts per million relative to DMSO-*d*<sub>6</sub>;  $^1\text{H}$ , 2.50 ppm and  $^{13}\text{C}$ , 39.5 ppm. The abbreviations in the script are as follows; im: imine and py: pyridyl. FTIR spectra were recorded using a Bruker Alpha FTIR spectrometer equipped with an ATR platinum Diamond 1 reflectance accessory. The instrument acquired the information in 32 scans with a spectral resolution of 1.0  $\text{cm}^{-1}$ . The abbreviations used in the script are as follows; s, strong; m, medium and w, weak signals. Electronic spectra were recorded using a Perkin Elmer Lambda 25 double-beam spectrophotometer (1.0 cm path length cuvette). Spectra were recorded from 700 to 200 nm in acetonitrile. High resolution mass spectra were determined with a Waters Acquity-LCT Premier coupled high performance liquid chromatograph-mass spectrometer (time-of-flight) using electrospray ionisation in positive mode.

The X-ray data were recorded on a Bruker Apex Duo diffractometer equipped with an Oxford Instruments Cryojet operating at 100(2) K and an Incoatec microsource operating at 30 W power. Crystal and structure refinement data are given in Table 1. In all four cases the data were collected with Mo K $\alpha$  ( $\lambda$  = 0.71073 Å) radiation at a crystal-to-detector distance of 50 mm. The data collections were performed using omega and phi scans with exposures taken at 30 W X-ray power and 0.50° frame widths using APEX2.<sup>34</sup> The data were reduced with the programme SAINT<sup>34</sup> using outlier rejection, scan speed scaling, as well as standard Lorentz and polarisation correction factors. A SADABS semi-empirical multi-scan absorption correction<sup>34</sup> was applied to the data. Direct methods, SHELXL-2014 (ref. 35) and WinGX<sup>36</sup> were used to solve all four structures. All non-hydrogen atoms were located in the difference density map and refined anisotropically with SHELXL-2014.<sup>29</sup> All hydrogen atoms were included as idealised contributors in the least squares process. Their positions were calculated using a standard riding model with C–H<sub>aromatic</sub> distances of 0.95 Å and  $U_{\text{iso}}$  = 1.2  $U_{\text{eq}}$ . Platon SQUEEZE<sup>37</sup> was used to remove disordered solvent from the lattice of complex  $[\text{Ag}-\mu\text{-(L3)}](\text{SbF}_6)$ . The process left solvent accessible voids of 884 Å<sup>3</sup>, which accounts for 18.3% of the unit cell volume.



**Scheme 1** Structure and naming scheme of the silver(I) complexes studied in this work.

### General procedure for the synthesis of $[\text{Ag}(\text{L1})](\text{SbF}_6)$ , $[\text{Ag}_2-\mu\text{-(L2)}_2](\text{SbF}_6)_2$ , $[\text{Ag}-\mu\text{-(L3)}](\text{SbF}_6)$ and $[\text{Ag}-\mu\text{-(L3)}](\text{BPh}_4)$

To a dry round-bottomed flask, two molar equivalents of pyridine-2-carboxaldehyde (312 mg, 2.91 mmol), one molar equivalent of the respective phenylenediamine regioisomers (157 mg, 1.45 mmol) and molecular sieves were added. Dry tetrahydrofuran (30 mL) was then added by cannula transfer and the solution heated to reflux. A yellow solution was observed after 30 minutes which was then transferred *via*

**Table 1** Summary of crystal data and structure refinement details for [Ag(L1)](SbF<sub>6</sub>), [Ag<sub>2</sub>-μ-(L2)]<sub>2</sub>(SbF<sub>6</sub>)<sub>2</sub>, [Ag-μ-(L3)](SbF<sub>6</sub>) and [Ag-μ-(L3)](BPh<sub>4</sub>)

Crystal data	[Ag(L1)](SbF <sub>6</sub> )	[Ag <sub>2</sub> -μ-(L2)] <sub>2</sub> (SbF <sub>6</sub> ) <sub>2</sub>	[Ag-μ-(L3)](SbF <sub>6</sub> )	[Ag-μ-(L3)](BPh <sub>4</sub> )
Chemical formula	C <sub>18</sub> H <sub>14</sub> AgF <sub>6</sub> N <sub>4</sub> Sb	C <sub>36</sub> H <sub>28</sub> Ag <sub>2</sub> F <sub>12</sub> N <sub>8</sub> Sb <sub>2</sub>	C <sub>18</sub> H <sub>14</sub> AgF <sub>6</sub> N <sub>4</sub> Sb	C <sub>42</sub> H <sub>34</sub> AgBN <sub>4</sub>
Molar mass g mol <sup>-1</sup>	629.95	1259.92	629.95	713.41
Crystal system, space group	Monoclinic, <i>P</i> <sub>2</sub> <sub>1</sub> / <i>n</i>	Monoclinic, <i>C</i> <sub>2</sub> / <i>c</i>	Monoclinic, <i>P</i> <sub>2</sub> <sub>1</sub> / <i>c</i>	Monoclinic, <i>P</i> <sub>2</sub> <sub>1</sub> / <i>c</i>
<i>a</i> , <i>b</i> , <i>c</i> /Å	7.7112(3), 12.8858(6), 19.6573(8)	16.2711(10), 15.9716(11), 15.6817(11)	13.6966(13), 13.1588(12), 26.895(3)	16.2241(15), 9.2420(9), 23.889(2)
$\beta$ /°	$\beta$ = 91.982(2)	$\beta$ = 102.447(3)	$\beta$ = 96.078(4)	$\beta$ = 107.447(2)
Temperature/K	100(2)	100(2)	100(2)	100(2)
<i>Z</i>	4	4	4	4
<i>V</i> /Å <sup>3</sup>	1952.08(14)	3979.5(5)	4820.1(5)	3417.2(6)
<i>F</i> (000)	1208.0	2416.0	2416	1464.0
$\mu$ /mm <sup>-1</sup>	2.455	2.409	1.99	0.626
Crystal Dim./mm	0.09 × 0.06 × 0.05	0.11 × 0.07 × 0.04	0.010 × 0.080 × 0.210	0.15 × 0.06 × 0.04
Data collection				
Total, unique data	5696, 5072	5303, 4950	11 340, 9294	6707, 5621
<i>R</i> <sub>int</sub>	0.0239	0.0264	0.0402	0.0250
Refinement				
Final Indices	<i>R</i> <sub>1</sub> = 0.024, <i>wR</i> <sub>2</sub> = 0.055	<i>R</i> <sub>1</sub> = 0.022, <i>wR</i> <sub>2</sub> = 0.049	<i>R</i> <sub>1</sub> = 0.091, <i>wR</i> <sub>2</sub> = 0.185	<i>R</i> <sub>1</sub> = 0.029, <i>wR</i> <sub>2</sub> = 0.070
<i>R</i> [ <i>I</i> > 2σ( <i>I</i> )]				

cannula to a second dry round-bottomed flask containing one molar equivalent silver(i) hexafluoroantimonate(v) (500 mg, 1.45 mmol) and the resulting solution stirred for 18 hours. The desired product precipitated from the solution as a pale green powder. The isolation, crystallisation and characterisation data for each complex are as follows.

#### 1,2-Bis(2-pyridyliminomethyl)benzene-silver(i) hexafluoroantimonate(v): [Ag(L1)](SbF<sub>6</sub>)

The product was separated from the reaction mixture by centrifugation and washed with THF, yielding a green powder (178 mg, 19.4% yield). Single crystals suitable for X-ray diffraction were grown by slow liquid diffusion of diethylether into a 2-methoxyethanol solution of the metal chelate. <sup>1</sup>H NMR (400 MHz, DMSO-*d*<sub>6</sub>, 303 K) [ $\delta$ , ppm]: 7.58 (m, 2H, NimCCH), 7.75 (m, 2H, NimCCHCH), 7.79 (m, 2H, NpyCHCH), 8.04 (d, 2H, NpyCCH), 8.21 (t of d, 2H, NpyCCHCH), 8.95 (d, 2H, NpyCH), 9.07 (s, 2H, NimCH). <sup>13</sup>C NMR (100 MHz, DMSO-*d*<sub>6</sub>, 303 K) [ $\delta$ , ppm]: 119.2 (NimCCH, NimCCHCH), 128.0 (NpyCHCH), 129.8 (NpyCCH), 139.7 (NpyCCHCH), 150.5 (NpyCH), 152.6 (NimCH). IR (cm<sup>-1</sup>): 649.60 (s, Sb-F), 771.86 (m, C-H out-of-plane bend), 1484.1, 1592.8 (m, C=C), 1629.3 (m, C=N). UV/vis (CH<sub>3</sub>CN) [ $\lambda$ <sub>max</sub>, nm;  $\epsilon$ , mol<sup>-1</sup> dm<sup>3</sup> cm<sup>-1</sup>]: 244; 2.10 × 10<sup>4</sup>, 300; 2.36 × 10<sup>4</sup>. ES<sup>+</sup> 393.03 *m/z* (M<sup>+</sup>).

#### $\mu$ -di(1,3-Bis(2-pyridyliminomethyl)benzene)-di-silver(i) hexafluoroantimonate(v): [Ag<sub>2</sub>-μ-(L2)]<sub>2</sub>(SbF<sub>6</sub>)<sub>2</sub>

The product was separated from the reaction mixture by centrifugation and washed with THF, resulting in a yellow-green powder (858 mg, 93.6% yield). Single crystals suitable for X-ray diffraction were grown by slow liquid diffusion of diethylether into an acetonitrile solution of the metal chelate. <sup>1</sup>H NMR (400 MHz, DMSO-*d*<sub>6</sub>, 303 K) [ $\delta$ , ppm]: 7.34 (d, 4H, NimCCH), 7.38 (s, 2H, NimCCHCNim), 7.46 (m, 2H,

NimCCHCH), 7.78 (m, 4H, NpyCHCH), 8.11 (d, 4H, NpyCCH), 8.20 (t of d, 4H, NpyCCHCH), 8.86 (d, 4H, NpyCH), 8.91 (s, 4H, NimCH). <sup>13</sup>C NMR (100 MHz, DMSO-*d*<sub>6</sub>, 303 K) [ $\delta$ , ppm]: 121.1 (NimCCH), 128.2 (NimCCHCNim, NimCCHCH), 130.8 (NpyCHCH, NpyCCH), 139.4 (NpyCCHCH), 150.9 (NpyCH), 151.6 (NimCH). IR (cm<sup>-1</sup>): 652.69 (s, Sb-F), 766.79 (m, C-H out-of-plane bend), 1480.5, 1593.0 (m, C=C), 1630.0 (m, C=N), 3061.0 (w, C-H). UV/vis (CH<sub>3</sub>CN) [ $\lambda$ <sub>max</sub>, nm;  $\epsilon$ , mol<sup>-1</sup> dm<sup>3</sup> cm<sup>-1</sup>]: 251; 4.70 × 10<sup>4</sup>, 281; 5.14 × 10<sup>4</sup>. ES<sup>+</sup> 393.03 *m/z* (M<sup>+</sup>).

#### catena-(μ-(1,4-Bis(2-pyridyliminomethyl)benzene)-silver(i) hexafluoroantimonate(v)) [Ag-μ-(L3)](SbF<sub>6</sub>)

The precipitate was separated from solution by centrifugation and washed with THF, giving a yellow-green powder (904 mg, 98.6% yield). Single crystals suitable for X-ray diffraction were grown by slow liquid diffusion of diethylether into an acetonitrile solution of the metal chelate. <sup>1</sup>H NMR (400 MHz, DMSO-*d*<sub>6</sub>, 303 K) [ $\delta$ , ppm]: 7.42 (s, 4H, NimCCH), 7.78 (m, 2H, NpyCHCH), 8.12 (d, 2H, NpyCCH), 8.19 (t of d, 2H, NpyCCHCH), 8.91 (d and s, 4H, NpyCH, NimCH). <sup>13</sup>C NMR (100 MHz, DMSO-*d*<sub>6</sub>, 303 K) [ $\delta$ , ppm]: 123.4 (NimCCH), 128.0 (NpyCHCH, NpyCCH), 139.3 (NpyCCHCH), 151.1 (NpyCH), 151.6 (NimCH). IR (cm<sup>-1</sup>): 653.10 (s, Sb-F), 837.36 (m, C-H out-of-plane bend), 1493.3, 1591.5 (s, C=C), 1620.6 (m, C=N), 3080.1 (w, C-H). UV/vis (CH<sub>3</sub>CN) [ $\lambda$ <sub>max</sub>, nm;  $\epsilon$ , mol<sup>-1</sup> dm<sup>3</sup> cm<sup>-1</sup>]: 236; 1.68 × 10<sup>4</sup>, 284; 1.79 × 10<sup>4</sup>, 354; 2.21 × 10<sup>4</sup>. ES<sup>+</sup> 393.03 *m/z* (M<sup>+</sup>).

#### catena-(μ-(1,4-Bis(2-pyridyliminomethyl)benzene)-silver(i) tetraphenylborate(m)) [Ag-μ-(L3)](BPh<sub>4</sub>)

Ammonium tetraphenylborate(v) was added to [Ag-μ-(L3)](SbF<sub>6</sub>) dissolved in acetonitrile (30 mL), and stirred for 72 hours. A light green precipitate was harvested by centrifugation, washed with a cold solution of acetonitrile

and dried, yielding in a yellow-green powder. Single crystals suitable for X-ray diffraction were grown by slow liquid diffusion of diethylether into an acetonitrile solution of the metal chelate.  $^1\text{H}$  NMR (400 MHz,  $\text{DMSO-}d_6$ , 298 K) [ $\delta$ , ppm]: 6.80 (t, 4H, BCHCHCH), 6.93 (m, 8H, BCHCH), 7.19 (t, 8H, BCH), 7.41 (s, 4H, NimCCH), 7.79 (m, 2H, NpyCHCH), 8.12 (d, 2H, NpyCCH), 8.20 (t of d, 2H, NpyCCHCH), 8.91 (d and s, 4H, NpyCH, NimCH).  $^{13}\text{C}$  NMR (100 MHz,  $\text{DMSO-}d_6$ , 303 K) [ $\delta$ , ppm]: 122.0 (BCHCHCH), 123.3 (NimCCH), 125.7 (BCHCH), 127.9 (NpyCHCH, NpyCCH), 136.0 (BCH), 139.2 (NpyCCHCH), 148.8 (NpyCH), 151.4 (NimCH). IR ( $\text{cm}^{-1}$ ): 701.21 (s, B–C stretch), 733.46 (s, C–H in plane bend), 838.21 (m, C–H out-of-plane bend), 1476.8, 1590.6 (m, C=C), 1621.5 (m, C=N), 2983.4, 3049.0 (m, C–H). UV/vis ( $\text{CH}_3\text{CN}$ ) [ $\lambda_{\text{max}}$ , nm;  $\epsilon$ ,  $\text{mol}^{-1} \text{dm}^3 \text{cm}^{-1}$ ]: 236;  $3.18 \times 10^4$ , 276;  $1.94 \times 10^4$ , 354;  $2.13 \times 10^4$ .  $\text{ES}^+$  393.03  $m/z$  ( $\text{M}^+$ ).

## Results and discussion

### NMR spectroscopy

The high symmetry of the compounds synthesised in this work lead to uncomplicated NMR spectra. All four compounds have the same chemical shift for the pyridyl hydrogen atoms of the bis(pyridyl-imine) ligands due to all pyridyl moieties having similar coordination modes. There are some differences with respect to the bridging units as a consequence of their varying degrees of symmetry. The imine C–H has a chemical shift of 9.07 ppm in  $[\text{Ag}(\text{L1})](\text{SbF}_6)$ , which is slightly further downfield compared to the imine C–H chemical shifts of  $[\text{Ag}_2\text{-}\mu\text{-(L2)}_2](\text{SbF}_6)_2$  and  $[\text{Ag-}\mu\text{-(L3)}]\text{X}$ , (where X =  $\text{BPh}_4^-$  or  $\text{SbF}_6^-$ ) all of which have chemical shifts of 8.91 ppm. This is attributed to the minor variations in the coordination geometries of the compounds:  $[\text{Ag}(\text{L1})](\text{SbF}_6)$  is square planar while the other compounds exhibit nominally tetrahedral coordination geometries. In the bridging moieties, compound  $[\text{Ag}(\text{L1})](\text{SbF}_6)$  has two chemical shifts, 7.58 ppm and 7.75 ppm, whereas compound  $[\text{Ag}_2\text{-}\mu\text{-(L2)}_2](\text{SbF}_6)_2$  has three chemical shifts, 7.37, 7.38 and 7.49 ppm; and compound  $[\text{Ag-}\mu\text{-(L3)}]\text{X}$  has only one chemical shift, 7.72 ppm. In the latter, the high symmetry of the compound leads to an equivalent chemical environment for the four phenyl C–H groups of the bridging unit. The  $^{13}\text{C}$  NMR data show similar patterns to those described above.

Silver(I) is known to be a labile metal ion and the structures elucidated in the solid-state may not be equivalent to those of the solution state. This is particularly true for L3, which forms a coordination polymer in the solid-state (*vide infra*). In an effort to confirm the identity of the species in solution, a simple titration experiment was performed as follows: 4.0 mg of L3 was dissolved in  $\text{DMSO-}d_6$  (0.5 mL) and the  $^1\text{H}$  NMR spectrum recorded and referenced according to the residual protonated  $\text{DMSO}$  at 2.50 ppm. A second stock solution of  $\text{AgSbF}_6$  was prepared by dissolving 4.8 mg of the salt (1 molar equivalent) in  $\text{DMSO-}d_6$  (0.5 mL). A 0.5 molar equivalent of  $\text{AgSbF}_6$  (0.25 mL of the stock solution) was added to the free ligand, and the  $^1\text{H}$  NMR spectrum recorded

after a five-minute incubation period at room temperature. A second aliquot comprising 0.5 molar equivalents was then added to give a 1:1 metal–ligand ratio and the  $^1\text{H}$  NMR spectrum again recorded after a five minute incubation period. The change in  $^1\text{H}$  NMR chemical shifts of the ligand with varying ratios of  $\text{AgSbF}_6$  in  $\text{DMSO-}d_6$  are shown in Fig. S11† (the free ligand spectrum is shown in Fig. S10†). The titration is interesting, indicating that the imine C–H and  $\alpha$ -pyridyl C–H switch positions (though maintain their multiplicity) upon chelation to the metal ion. Although the chemical shifts of both move downfield, the imine C–H moves further downfield, past the chemical shift for the  $\alpha$ -pyridyl C–H. Importantly, the chemical shifts at the end of the titration match those observed when a crystalline sample of  $[\text{Ag-}\mu\text{-(L3)}](\text{SbF}_6)$  is dissolved in  $\text{DMSO-}d_6$ . These spectra show that metal ion chelation occurs in solution, even in coordinating solvent. It is therefore likely, the species observed in the solid-state is also found in the solution state. Due to the electron-withdrawing effects of the metal ion, the chemical shifts of all hydrogen atoms move downfield; deshielded by the electron-withdrawing silver(I). As the coordination polymer formed between L3 and silver(I) is likely to be the least stable species in solution, it is probable that the solid-state structures  $[\text{Ag}(\text{L1})](\text{SbF}_6)$  and  $[\text{Ag}_2\text{-}\mu\text{-(L2)}_2](\text{SbF}_6)_2$  are similarly stable in solution.

Fully assigned  $^1\text{H}$  and  $^{13}\text{C}$  NMR spectra are available in the electronic ESI.†

### UV-visible spectroscopy

The electronic transitions of all three complexes are dominated purely by ligand-based  $\pi \rightarrow \pi^*$  and  $n \rightarrow \pi^*$  transitions as the silver(I) ion with a  $d^{10}$  electron configuration precludes participation of the metal ion from electronic transitions. Hence the absence of lower-energy metal-to-ligand charge transfer bands, typically located between 400–450 nm. All spectra were recorded in acetonitrile giving visibly colourless solutions; this being justified by the absorption bands outside of the visible region of the electromagnetic spectrum. Despite the lack of participation by the metal ion, each complex has unique absorption bands attributed to the variable structures of the bis(pyridyl-imine) ligands and their corresponding metal complexes. The spectra show increased resolution of the absorption bands as well as a bathochromic shift as a function of positional substitution (Fig. 1).

### Solid-state structures of $[\text{Ag}(\text{L1})](\text{SbF}_6)$ , $[\text{Ag}_2\text{-}\mu\text{-(L2)}_2](\text{SbF}_6)_2$ , $[\text{Ag-}\mu\text{-(L3)}](\text{SbF}_6)$ and $[\text{Ag-}\mu\text{-(L3)}](\text{BPh}_4)$

All four complexes were studied by single crystal X-ray diffraction. Each ligand was coordinated to silver(I) using silver(I) hexafluoroantimonate(V) as the source of metal ions in a 1:1 metal/ligand ratio. In addition, the counter anion of chelate  $[\text{Ag-}\mu\text{-(L3)}](\text{SbF}_6)$  was exchanged for a bulkier tetraphenylborate(V) counter anion during synthesis to reduce

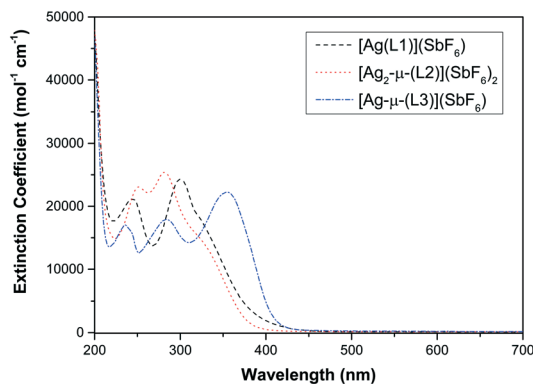


Fig. 1 Electronic spectra of  $[\text{Ag}(\text{L1})](\text{SbF}_6)$ ,  $[\text{Ag}_2-\mu-(\text{L2})](\text{SbF}_6)_2$ ,  $[\text{Ag}-\mu-(\text{L3})](\text{SbF}_6)$  showing improved resolution and bathochromic shift in the order *ortho* < *meta* < *para* in terms of increased resolution and extent of bathochromic shift.

the solvent accessible volume and hence yield a more stable crystal lattice.

The silver chelate  $[\text{Ag}(\text{L1})](\text{SbF}_6)$  crystallised in the monoclinic space group  $P2_1/n$ . The asymmetric unit (Fig. 2) consists one independent silver(i) chelate and hexafluoroantimonate(v) counter anion, and  $Z = 4$ . The chelate is monomeric with one metal ion coordinated to the tetradentate bis(pyridyl-imine) ligand through the two *cis*-pyridyl and two *cis*-imine nitrogen atoms of the complex. The monomeric chelate shows a moderately planar structure, this is the expected geometry of the ligand. Any significant deviation from planarity would impede the  $\pi$ -conjugation of the ligand making it less stable. The ligand donor set is thus primed for square planar coordination. Correspondingly, the metal ion has adopted a nominally square planar coordination geometry with the silver(i) ion very slightly displaced, 0.043 Å, from the four-atom mean plane defined by the coordinating atoms. The bond lengths and bond angles describing the coordination sphere are summarised in

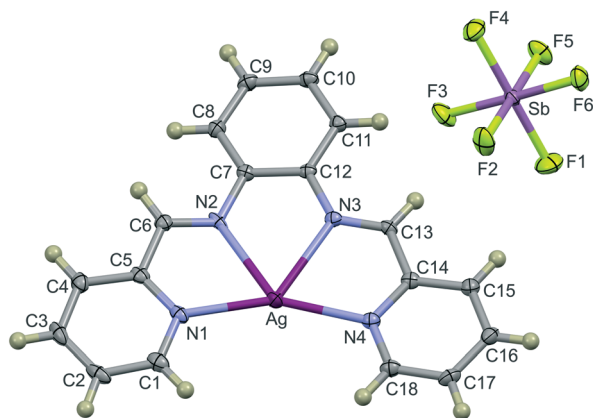


Fig. 2 Thermal ellipsoid plot (50% probability level) of  $[\text{Ag}(\text{L1})](\text{SbF}_6)$ , showing the approximately square planar coordination geometry of the metal ion and the atom numbering scheme of the asymmetric unit. Hydrogen atoms are rendered as spheres of arbitrary radius.

Table 2. The rigid two-carbon di(azomethine) bridging unit renders a constrained ligand bite and hence the N2–Ag–N3 bond angle is significantly acute measuring  $64.71(6)^\circ$ . Consequently, the N1–Ag–N4 bond angle is obtuse, measuring  $154.40(6)^\circ$ . The  $N_{\text{pyridyl}}\text{--Ag--}N_{\text{imine}}$  bond angles are approximately equal with a mean value of  $70.58(8)^\circ$ . The strained coordination geometry leads to significant differences in the  $N_{\text{pyridyl}}\text{--Ag}$  and  $N_{\text{imine}}\text{--Ag}$  bond lengths, which average  $2.243(3)$  and  $2.461(3)$  Å, respectively.

The compound shows evidence of a range of intermolecular interactions including  $\text{Ag}\cdots\text{Ag}$ ,  $\text{Ag}\cdots\pi$  and  $\pi\cdots\pi$  contacts. The compound packs as inversion dimers stabilised by  $\text{Ag}\cdots\text{Ag}$  and  $\pi\cdots\pi$  interactions (Fig. 3). It would seem that these interactions are moderately strong as the interplanar spacing of the molecules is 3.236 Å. This distance is significantly shorter than the interplanar spacing in the  $\pi$ -system of graphite: 3.35 Å. The inversion dimers are then linked by additional, similar interactions leading to one-dimensional  $\pi$ -stacked columns. The  $\text{Ag}\cdots\text{Ag}$  separation of these close-packed columns measures  $3.8497(3)$  Å.

Ligand L2 is an interesting case. The arrangement of the ligand donor set precludes the formation of a monomeric species due to the position of C10–H10 unit, a multi-nuclear structure is therefore anticipated. When the ligand L2 and metal are reacted in a 1:1 ratio, the compound  $[\text{Ag}_2-\mu-(\text{L2})](\text{SbF}_6)_2$  forms, crystallising in the monoclinic space group  $C2/c$ . The structure is an unusual dimetallic chelate with two silver(i) ions bridged by two ligands. The asymmetric unit (Fig. 4) comprises a single ligand and metal ion with an associated hexafluoroantimonate(v) anion. The asymmetric unit is the substructure of the dimetallic, ligand-bridged species which has inversion symmetry, thus  $Z = 4$ . The rigid aromatic bis(imine) ligand bridging unit with 1,3-diamino substitution is seemingly pre-organised for formation of a dinuclear complex. The silver(i) ions have a distorted tetrahedral coordination geometry. This distorted coordination geometry has allowed the adjacent bridging phenyl rings to be co-planar. This co-planar arrangement supports  $\pi\cdots\pi$  interactions which further stabilise the metal complex by *ca.* 11  $\text{kJ mol}^{-1}$  (*vide infra*). The mean plane separation of the two  $\pi$ -systems is 3.334 Å. This is comparable to the mean plane separation of graphite (3.35 Å) and the interaction is therefore likely to be moderately strong. Structural parameters for all four complexes are found in Table 2.

It is noteworthy that the two silver(i) atoms in the dimetallic structure are separated by a distance of  $8.5247(6)$  Å, which is significantly different to the distance reported in the work done by Deng *et al.*:  $13.0170(7)$ , which is similarly a *meta*-substituted, ligand-bridged dinuclear silver(i) species.<sup>19</sup> Changing the bridging unit, from a flexible bis(pyridyl-imine) to a semi-rigid bis(pyridyl-imine), alters the crystal structure significantly. The less flexible ligand presented ligand herein should be a more predictable entity for use in crystal engineering. The  $\text{Ag}\cdots\text{Ag}$  separation is, however, longer than that reported by Pandey *et al.*:  $7.905(2)$  Å.<sup>38</sup> The inductive effects of the trimethyl substitution on the phenyl

**Table 2** Bond lengths (Å) and bond angles (°) for compounds [Ag(L1)](SbF<sub>6</sub>), [Ag<sub>2</sub>-μ-(L2)<sub>2</sub>](SbF<sub>6</sub>)<sub>2</sub>, [Ag-μ-(L3)](SbF<sub>6</sub>)<sup>a</sup>, and [Ag-μ-(L3)](BPh<sub>4</sub>). Standard uncertainties are given in parentheses

Bond lengths (Å)		Compound			
Bond	[Ag(L1)](SbF <sub>6</sub> )	[Ag <sub>2</sub> -μ-(L2) <sub>2</sub> ](SbF <sub>6</sub> ) <sub>2</sub>	[Ag-μ-(L3)](SbF <sub>6</sub> ) <sup>a</sup>	[Ag-μ-(L3)](BPh <sub>4</sub> )	
N1–Ag1	2.240(2)	2.221(2)	2.322(9)	2.239(2)	
N2–Ag1	2.457(2)	2.458(2)	2.313(9)	2.471(2)	
N3–Ag1	2.464(2)	2.434(2)	2.320(9)	2.413(2)	
N4–Ag1	2.245(2)	2.239(2)	2.330(8)	2.297(2)	
Bond angles (°)		Compound			
Bond	[Ag(L1)](SbF <sub>6</sub> )	[Ag <sub>2</sub> -μ-(L2) <sub>2</sub> ](SbF <sub>6</sub> ) <sub>2</sub>	[Ag-μ-(L3)](SbF <sub>6</sub> ) <sup>a</sup>	[Ag-μ-(L3)](BPh <sub>4</sub> )	
N1–Ag1–N2	70.39(6)	72.11(6)	72.3(3)	72.01(6)	
N2–Ag1–N3	64.71(6)	84.69(6)	107.3(3)	105.41(6)	
N3–Ag1–N4	70.76(6)	72.12(6)	72.7(3)	72.27(6)	
N1–Ag1–N4	154.4(6)	151.74(7)	132.9(3)	139.01(7)	

<sup>a</sup> Mean values for the two independent molecules in the asymmetric unit.

bridge reported by Pandey *et al.* may assist with the formation of the shorter bond distance (Fig. 5).

Two pseudopolymorphs of [Ag-μ-(L3)] (x) were synthesised and crystallised, where x = either SbF<sub>6</sub><sup>-</sup> or BPh<sub>4</sub><sup>-</sup>. (Fig. 6 and 7). When crystallised with an SbF<sub>6</sub><sup>-</sup> anion, the crystal lattice contains significant solvent accessible voids occupied by numerous disordered acetonitrile solvent molecules. The solvent molecules were removed *in silico* using Platon SQUEEZE.<sup>37</sup> The void contact surface was calculated using a probe of 1.2 Å radius, indicating [Ag-μ-(L3)](SbF<sub>6</sub>) has solvent accessible volumes of 884 Å<sup>3</sup>, *i.e.* 18.4% of the unit cell volume. The chelate [Ag-μ-(L3)](SbF<sub>6</sub>) crystallised in the monoclinic space group *P*2<sub>1</sub>/*c*. The asymmetric unit (Fig. 6) comprises two symmetry-independent ligands each coordinated to a silver(i) ion through one imine and one

pyridyl nitrogen atom. The linear structure of the ligand promotes the formation of a coordination polymer (Fig. 6 inset). The two molecules in the asymmetric unit are

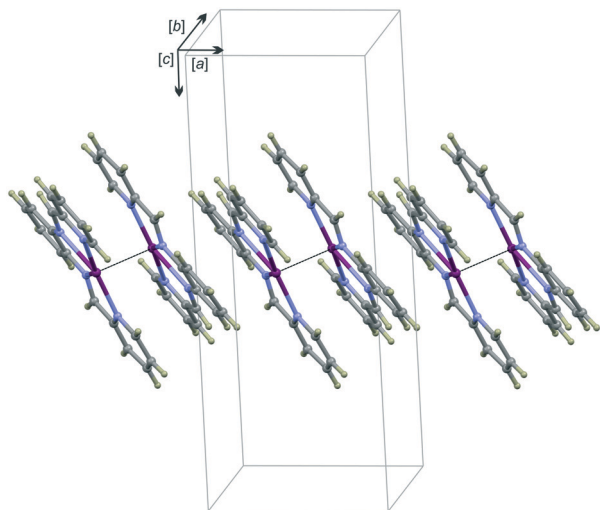


**Fig. 3** Dimeric structures related through crystallographic inversion symmetry, stabilised by Ag...Ag and π...π interactions, are linked together through additional π...π and Ag...π interactions to form one-dimensional columns. The Ag...Ag separation of the dimers measures 3.8497(3) Å and is indicated on the diagram as a dashed, black line. Symmetry code: 1 - x, 1 - y, 1 - z.

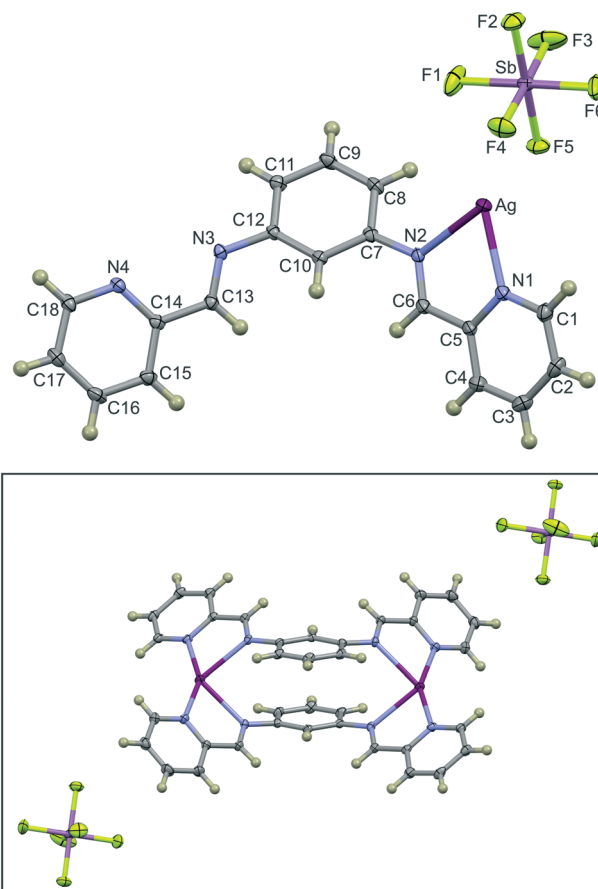


**Fig. 4** [Main] Thermal ellipsoid plot (50% probability level) of the asymmetric unit of [Ag<sub>2</sub>-μ-(L2)<sub>2</sub>](SbF<sub>6</sub>)<sub>2</sub>, showing the atom numbering scheme. [Inset] The symmetry-completed dimetallic structure showing the co-planar bridging phenyl rings and approximately tetrahedral coordination geometry of the metal ion. Hydrogen atoms are rendered as spheres of arbitrary radius. Symmetry code: (i) -x, -y, -z.

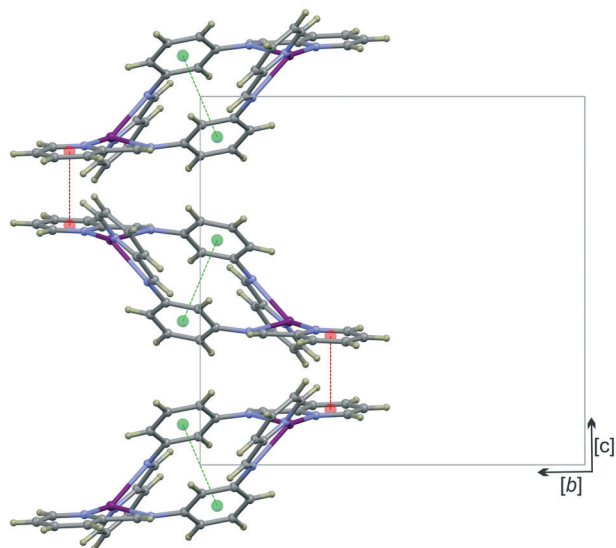


**Fig. 5** One-dimensional chain (viewed down  $[a]$ ) of  $[\text{Ag}_2\text{-}\mu\text{-(L2)}_2](\text{SbF}_6)_2$ ; the chain is co-linear with the  $c$ -axis supported by  $\pi\cdots\pi$  interactions. The intermolecular and intramolecular  $\pi\cdots\pi$  interactions are shown in green and red, respectively. Anions have been omitted for clarity, and all atoms are shown as spheres of arbitrary radius. This illustrates the influence of non-covalent interactions in crystal engineering as described in previous works.<sup>28–33</sup>

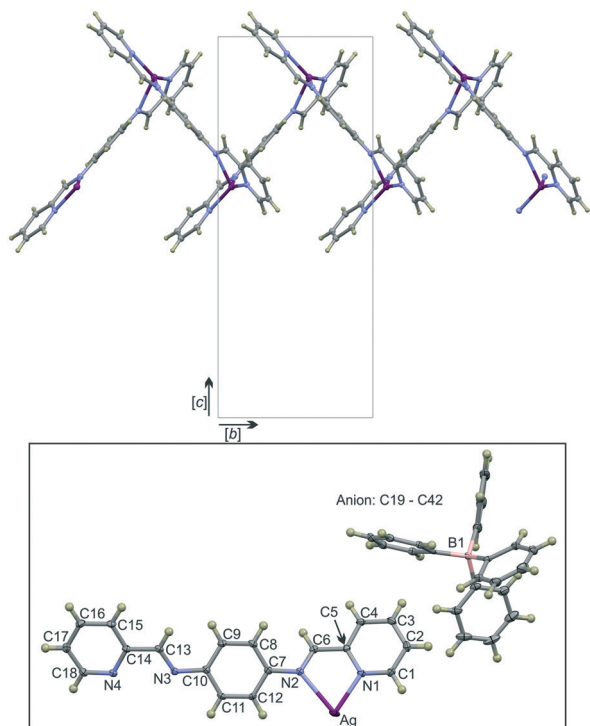


**Fig. 6** [Main] Thermal ellipsoid plot (50% probability level) of the asymmetric unit of  $[\text{Ag-}\mu\text{-(L3)}](\text{SbF}_6)$ , showing the atom numbering scheme. Hydrogen atoms are rendered as spheres of arbitrary radius. [Inset] The symmetry-completed coordination polymer. Note that the two molecules in the asymmetric unit are stabilised by  $\pi\cdots\pi$  interactions (shown in red), but each propagates an independent chain of molecules (coordination polymers). Symmetry code: (i)  $x, y, z$ .

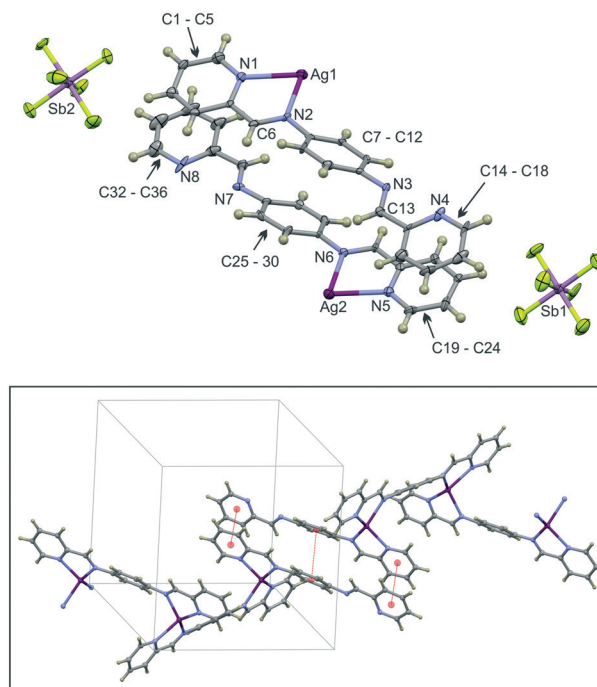


**Fig. 7** [Main] The symmetry-completed coordination polymer of  $[\text{Ag-}\mu\text{-(L3)}](\text{BPh}_4)$  viewed down the  $a$ -axis, the counterions have been omitted for clarity. The coordination polymer is col-linear with the  $b$ -axis. All atoms are shown as spheres of arbitrary radius. [Inset] Thermal ellipsoid plot (50% probability level) of the asymmetric unit of  $[\text{Ag-}\mu\text{-(L3)}](\text{SbF}_6)$ , showing the atom numbering scheme. Hydrogen atoms are rendered as spheres of arbitrary radius. Symmetry code: (i)  $1 - x, \frac{1}{2} + y, 1.5 - z$ .

similar in geometry and each propagates a coordination polymer. The coordination geometry of the silver(i) ion is a distorted tetrahedron; this leads to a herringbone pattern for the coordination polymer. The relative rotation of the ligands forming the coordination polymer is best described by the N1–Ag1–N3–C10 torsion angle which measures  $37.3(8)^\circ$  and N7–Ag2–N5–C23 which measures  $35.7(6)^\circ$ . The two nine-atom mean planes each comprising the pyridyl–imine moiety and silver ion form angles of approximately  $63^\circ$  for each independent polymer.

Despite the extended  $\pi$ -conjugation of the ligands, the ligands are not planar as may be expected. The two pyridyl rings of each ligand are co-planar, but show a relative rotation with respect to the bridging phenyl ring. This non-planarity is illustrated by the angles subtended by the four eight-atom mean planes each comprising the pyridyl–imine moiety and the two six-atom mean planes of the bridging phenyl rings. The mean of the four angles is  $35(4)^\circ$ . These angles are the biggest difference between the two molecules in the asymmetric unit. In molecule 1, the two pyridyl imine groups form a mean angle of  $31.3(2)$  and in molecule two, the equivalent angle subtended by these groups measures  $39.3(6)^\circ$ . The Ag $\cdots$ Ag separations are  $7.925(1)$  and  $7.912(1)$  Å for the Ag1 $\cdots$ Ag1 and Ag2 $\cdots$ Ag2 coordination polymers, respectively.

As described above, the crystal lattice of  $[\text{Ag}-\mu\text{-(L3)}](\text{SbF}_6)$  has large solvent-accessible channels occupied by disordered acetonitrile. The relatively volatile solvent would exit the channels during crystal mounting and data collection, lowering the quality of the data as sample crystallinity was concomitantly lost. To stabilise the lattice and potentially reduce the size of the channels in the lattice, the counter anion was switched from  $\text{SbF}_6^-$  to  $\text{BPh}_4^-$  (the asymmetric unit of  $[\text{Ag}-\mu\text{-(L3)}](\text{BPh}_4)$  is shown in Fig. 7). This still allowed for formation of the coordination polymer (Fig. 7). However, the anionic molecules now occupied the channels in the lattice (Fig. 8) and reduced the solvent accessible surface from  $884 \text{ \AA}^3$ , 18.4% of the unit cell volume, (calculated using a  $1.2 \text{ \AA}$  radius probe) to  $33.7 \text{ \AA}^3$ , *i.e.* 1.0% of the unit cell volume when calculated using the same probe radius. A comparison of the solvent-accessible voids is shown in Fig. 9. This slightly modified chelate  $[\text{Ag}-\mu\text{-(L3)}](\text{BPh}_4)$  still crystallised in the same space group,  $P2_1/c$ , however, the asymmetric unit (Fig. 7) now consists of a single chelate and tetraphenylborate(III) counter anion.

Fig. 7 and the data in Table 2 show the silver(I) ion again adopts a distorted tetrahedral coordination geometry in  $[\text{Ag}-\mu\text{-(L3)}](\text{BPh}_4)$  with the coordination sphere comprising four nitrogen atoms (two pyridyls and two imines) from two independent ligands. Thus, each silver ion bridges two ligands and each ligand bridges two silver ions. This leads to a one-dimensional coordination polymer. In this case, the ligands of the coordination polymer more closely approach a perpendicular orientation as illustrated by the N1–Ag1–N3–C10 torsion angle, which measures  $74.6(2)^\circ$ . The ligand again deviates from planarity, the consistent deviation from planarity despite the extended  $\pi$ -conjugation suggests that the destabilising effect caused by the ligand twisting is perhaps offset by the energy gains of more favourable metal ion chelation and the formation of supramolecular structures. The

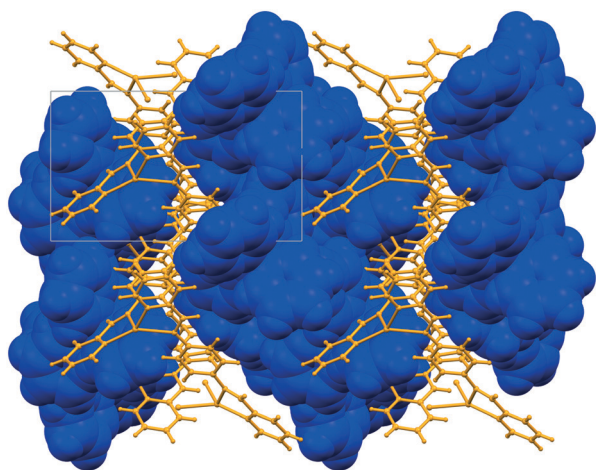


Fig. 8 Packing of  $[\text{Ag}-\mu\text{-(L3)}](\text{BPh}_4)$  viewed down the *c*-axis. The anionic  $\text{BPh}_4^-$  ions are rendered using their van der Waals radii and are coloured blue. The coordination polymers are shown as spheres of an arbitrary radius in yellow. This highlights the alternating layers of polymer chains and anions which leads to a stable crystal lattice.

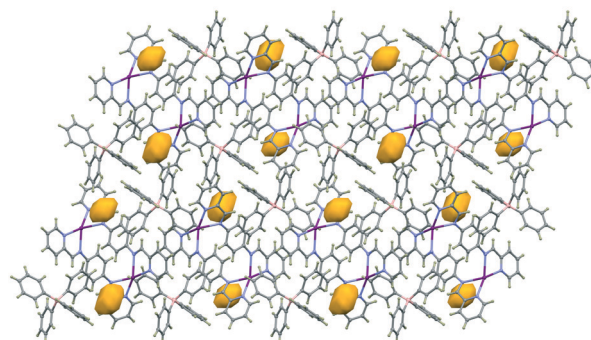
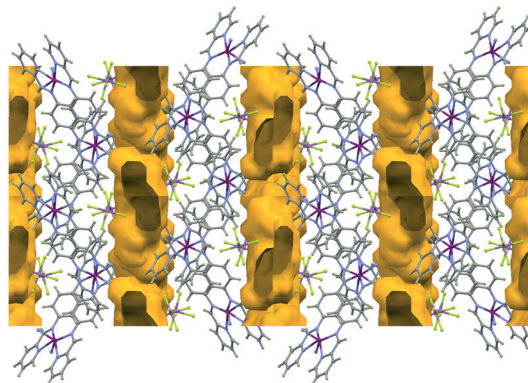


Fig. 9 A comparison of solvent-accessible voids for chelates [top]  $[\text{Ag}-\mu\text{-(L3)}](\text{SbF}_6)$  and [bottom]  $[\text{Ag}-\mu\text{-(L3)}](\text{BPh}_4)$ . The volume and structure of the voids are changed through exchanging the counterions. The latter structure is thus also more stable.

deviation from planarity in the case of  $[\text{Ag}-\mu\text{-(L3)}](\text{BPh}_4)$  is illustrated by the relative rotations of the terminal pyridyl rings with respect to the bridging phenyl ring. The six-atom mean planes comprising N1, C1–C5, and N4, C14–C18, subtend angles relative to the six-atom mean plane of the bridging phenyl ring, C7–C12, of  $24.9$  and  $15.7^\circ$ , respectively.

Upon exchanging the counter anion of chelate  $[\text{Ag}-\mu\text{-(L3)}](\text{SbF}_6)$  from hexafluoroantimonate(V) to tetraphenylborate(V), a polymeric structure was once again formed. This is significant as it shows that the formation of coordination polymers is favoured under different reaction conditions. By replacing  $\text{SbF}_6^-$ , which has a relatively small molecular volume when compared with  $\text{BPh}_4^-$ , the result is alternating layers of coordination polymers and anions as shown in Fig. 8.

Although significantly smaller, this polymeric chelate once again contains voids in the lattice, with a contact surface of  $33.71 \text{ \AA}^3$  (Fig. 9). This is likely attributed to the larger tetraphenylborate(III) counter ions occupying more space; driving the solvent void pockets to be smaller.

The most notable feature of all four compounds is the variation in bond angles as a consequence of the restrained ligand bite and changes in coordination geometry. The angle between the imine nitrogen atoms, N2–Ag–N3, varies significantly as a function of the aromatic bridging unit structure *ortho*- < *meta*- < *para*-. This change in bond angle also reflects the change from an approximately square planar

coordination geometry in the case of *ortho*-substitution to nominally tetrahedral in the case of *para*-substitution. Correspondingly, the angle subtended by the pyridyl N-donor atoms, N1–Ag1–N4, decrease significantly: *ortho* > *meta* > *para*. The trend in bond lengths is the same for all compounds in this series with the Ag–N<sub>pyridyl</sub> bond lengths being considerably shorter than the Ag–N<sub>imine</sub> bond lengths. The mean bond lengths for the four Ag–N<sub>pyridyl</sub> and Ag–N<sub>imine</sub> bonds are 2.27(4) and 2.42(6) Å, respectively. These bond length and bond angles are comparable to those of related structures.<sup>38–45</sup>

### Molecular simulations

Density functional theory (DFT) simulations were used to gain a deeper understanding of the solid-state structures and associated energies of the silver(I) chelates. The simulations were performed using Gaussian 09W<sup>46</sup> using the PBE hybrid functional.<sup>47,48</sup> A split basis set was applied in the simulations, this split basis set specified the 6-311G(dp) level of theory<sup>49,50</sup> for the C, H, and N atoms and the LanL2DZ (which makes use of effective core potentials) basis set for the silver(I) ion.<sup>51–54</sup> The X-ray coordinates of the metal chelates were used for input structures. Normal geometry convergence criteria were applied and no symmetry constraints imposed. The input files were prepared using GaussView 5.0;<sup>55</sup> the same program was used to analyse the output files. Structural overlays were performed using Mercury 2020, v. 2.0.<sup>56</sup>

The rigid structure of L1 and the correspondingly predictable structure of [Ag(L1)](SbF<sub>6</sub>) could be accurately simulated. The root-mean-square deviation (RMSD) for the least-squares fit of all atoms in the structure is 0.1814 Å showing good correlation between the structures. The rigidity of the ligand and few degrees of freedom allow for accurate structure simulation *in vacuo*. This also shows the intermolecular interactions in the solid state have little influence on the molecular geometry. The least squares fit is shown in Fig. S22.†

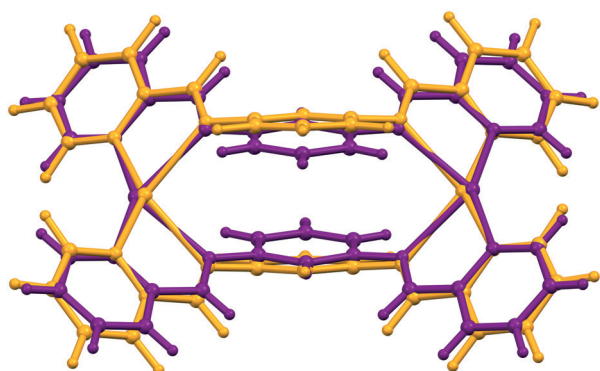


**Fig. 10** Least-squares-fit of the geometry-optimised (yellow) and experimental (purple) structures of [Ag<sub>2</sub>-μ-(L<sub>2</sub>)<sub>2</sub>](SbF<sub>6</sub>)<sub>2</sub> showing the shorter Ag...Ag separation and larger spacing between the bridging phenyl rings. The π...π interaction between the bridging phenyl rings stabilises the molecule by ca. 11 kJ mol<sup>-1</sup>.

The compound [Ag<sub>2</sub>-μ-(L<sub>2</sub>)<sub>2</sub>](SbF<sub>6</sub>)<sub>2</sub> is similarly rigid, but does show more structural deviation between the simulated and experimental geometries (Fig. 10). The Ag...Ag distance in the complex [Ag<sub>2</sub>-μ-(L<sub>2</sub>)<sub>2</sub>](SbF<sub>6</sub>)<sub>2</sub> is 8.091 Å for the geometry-optimised structure. This is significantly shorter than the experimental structure: 8.5247(6) Å. Conversely, the interplanar spacing of the phenyl bridging units is increased in the optimised form with a distance of 3.866 Å between the two six-atom mean planes. These geometric parameters show that the compound has, in a sense been compressed, bringing the silver(I) ion closer and forcing the π-systems further apart. Through comparison of the geometry-optimised monomeric and dimeric structures, it is evident the π...π interaction of the bridging unit stabilises the structure by ca. 10.7 kJ mol<sup>-1</sup>. Despite the differences described above, there is relatively good agreement between the geometry-optimised and experimental data with a least-squares-fit of all atoms yielding a root-mean-square-deviation (RMSD) of 0.3211 Å (Fig. 10).

The polymeric nature of [Ag-μ-(L<sub>3</sub>)](x) complicates the geometry-optimisation process. A trimeric sub-structure of the coordination polymer was used as a representative example in the geometry optimisation (Fig. S23†). The least squares fit of the bridging ligand shows that in the absence of steric restraints imposed by the crystal lattice, the geometry-optimised structure has the ligands subtending an angle of ca. 90°. This is in contrast to the experimental structures which subtend angles of approximately 65–75°.

## Conclusions

A series of *ortho*-, *meta*- and *para*-substituted phenylene-bridged silver(I) bis(pyridyl-imine) complexes have been successfully synthesised in facile a two-step process yielding three structurally distinct complexes as a consequence of ligand donor atom pre-organisation. Due to the pre-organised architecture of the di(azomethine) linkage in each ligand, monomeric, dimeric and polymeric structures were synthesised. Ligand 1,2-bis(2-pyridyliminomethyl)benzene (L1) forms a monomeric complex, [Ag(L1)](SbF<sub>6</sub>), ligand 1,3-bis(2-pyridyliminomethyl)benzene (L2) forms a dimeric complex [Ag<sub>2</sub>-μ-(L<sub>2</sub>)<sub>2</sub>](SbF<sub>6</sub>)<sub>2</sub>, and ligand 1,4-bis(2-pyridyliminomethyl)benzene (L3) forms a polymeric complex [Ag-μ-(L<sub>3</sub>)](SbF<sub>6</sub>). The latter coordination polymer was found to be robust with respect to the counter anion; both [Ag-μ-(L<sub>3</sub>)](SbF<sub>6</sub>) and [Ag-μ-(L<sub>3</sub>)](BPh<sub>4</sub>) form polymeric structures in the solid state. The d<sup>10</sup> electronic configuration of silver(I) and lack of CFSE (and therefore no strong preference for coordination geometry) allowed for both tetrahedral and square planar coordination environments. This was necessary to form the different monomeric and supramolecular structures. These examples show the potential of ligand donor atom pre-organisation for application in crystal engineering.

## Conflicts of interest

There are no conflicts to declare.

## Acknowledgements

The authors gratefully acknowledge the University of KwaZulu Natal for their financial support and use of facilities as well as the National Research Foundation (South Africa) for their financial funding. The Authors would also like to thank Mr Craig Grimmer for the recording of the NMR spectra.

## Notes and references

- B. Moulton and M. J. Zaworotko, *J. Chem. Rev.*, 2001, **101**, 1629–1658.
- M. Shyamal, A. Panja and A. Saha, *Polyhedron*, 2014, **69**, 141–148.
- M. O. Awaleh, F. Brisse, Y. D. Soubaneh, T. Maris and E. S. Dirieh, *J. Inorg. Organomet. Polym.*, 2010, **20**, 816–824.
- T. G. Campbell and F. L. Urbach, *Inorg. Chem.*, 1973, **12**, 1836–1840.
- P. G. Cozzi, *Chem. Soc. Rev.*, 2004, **33**, 410–421.
- S. Kuma, D. N. Dhar and P. N. Saxena, *J. Sci. Ind. Res.*, 2009, **68**, 181–187.
- Z. Shir-Yeta and M. R. Yaftian, *Iran. J. Chem. Chem. Eng.*, 2010, **29**, 11–17.
- M. P. Akerman, O. Q. Munro, M. Mongane, J. A. van Staden, W. I. D. Rae, C. J. Bester, B. Marjanovic-Painter, Z. Szucs and J. R. Zeevaart, *J. Labelled Compd. Radiopharm.*, 2013, **56**, 530–535.
- K. J. Akerman, A. M. Fagenson, V. Cyril, M. Taylor, M. T. Muller, M. P. Akerman and O. Q. Munro, *J. Am. Chem. Soc.*, 2014, **136**, 5670–5682.
- I. Ebraliidze, G. Leitus, L. J. W. Shimon, Y. Wang, S. Shaik and R. Neumann, *Inorg. Chim. Acta*, 2009, **362**, 4713–4720.
- R. Zhang, J. Zhao, P. Yang and Q. Shi, *J. Chem. Crystallogr.*, 2010, **40**, 357–368.
- A. Pajunen and S. Panjunen, *Acta Crystallogr., Sect. C: Cryst. Struct. Commun.*, 1986, **42**, 53–56.
- A. Panja, *Polyhedron*, 2014, **80**, 81–89.
- S. Striegler and M. Dittel, *J. Am. Chem. Soc.*, 2003, **125**, 11518–11524.
- M. Mikuriya, Y. Hatano and E. Asato, *Bull. Chem. Soc. Jpn.*, 1997, **70**, 2495–2507.
- M. P. Akerman, T. Chatturgoon and O. Q. Munro, *Inorg. Chim. Acta*, 2014, **421**, 292–299.
- Z. Zhang, Z. Deng, L. Huo, H. Zhao and S. Gao, *Inorg. Chem.*, 2013, **52**, 5914–5923.
- J. Huang, Z. Deng, Y. Xiao, L. Huo, S. Zhao, F. Ge and S. Gao, *Dalton Trans.*, 2015, **44**, 5837–5847.
- Z. Deng, L. Zhu, S. Gao, L. Huo and S. W. Ng, *Cryst. Growth Des.*, 2008, **9**, 3277–3284.
- Q. I. Zhang, P. Hu, Y. Zhao, Q.-W. Feng, Y.-Q. Zhang, B.-X. Zhu and Z. J. Tao, *J. Solid State Chem.*, 2014, **210**, 178–187.
- M. Tsiouri, J. C. Plakatouras, A. Garoufis, V. Nastropoulos and N. Hadjiliadis, *Inorg. Chem. Commun.*, 2002, **5**, 844–847.
- A. Garoufis, S. Kasselouri, C. Mitsopoulou, J. Sletten, C. Papadimitriou and N. Hadjiliadis, *Polyhedron*, 1999, **18**, 39–47.
- C. Giri, F. Topic, P. Mal and K. Rissanen, *Dalton Trans.*, 2014, **43**, 15697–15699.
- N. Chanda, B. Mondal, V. G. Puranik and G. K. Lahiri, *Polyhedron*, 2002, **21**, 2033–2043.
- G. Li, Y. Wu, G. Shan, W. Che, D. Zhu, B. Song, L. Yan, Z. Su and M. R. Bryce, *Chem. Commun.*, 2014, **50**, 6977–6980.
- A. Hasheminasab, J. T. Engle, J. Bass, R. S. Herrick and C. J. Ziegler, *Eur. J. Inorg. Chem.*, 2014, 2643–2652.
- Y. Wang, H. Fu, A. Peng, Y. Zhao, J. Ma, Y. Ma and J. Yao, *Chem. Commun.*, 2007, 1623–1625.
- S. Tripathi, S. Islam, S. K. Seth, A. Bauzá, A. Frontera and S. Mukhopadhyay, *CrystEngComm*, 2020, **22**, 8171–8181.
- G. Mahmoudi, S. K. Seth, A. Bauzá, F. I. Zubkovd, A. V. Gurbanove, J. Whiteg, V. Stilinovič, T. Doerti and A. Frontera, *CrystEngComm*, 2018, **20**, 2812–2821.
- S. K. Seth, A. Bauzá and A. Frontera, *CrystEngComm*, 2018, **20**, 746–754.
- S. K. Seth, A. Bauza and A. Frontera, *New J. Chem.*, 2018, **42**, 12134–12142.
- A. Bauzá, S. K. Seth and A. Frontera, *Coord. Chem. Rev.*, 2019, **384**, 107–125.
- S. K. Seth, A. Bauzá, G. Mahmoudi, V. Stilinović, E. López-Torres, G. Zaragoza, A. D. Keramidag and A. Frontera, *CrystEngComm*, 2018, **20**, 5033–5044.
- Bruker, *APEX2, SAINT and SADABS*, Bruker AXS Inc., Madison, Wisconsin, USA, 2012.
- G. M. Sheldrick, *Acta Crystallogr., Sect. C: Struct. Chem.*, 2015, **71**, 3–8.29.
- L. J. Farrugia, *J. Appl. Crystallogr.*, 2012, **45**, 849–854.
- A. L. Spek, *Acta Crystallogr., Sect. D: Biol. Crystallogr.*, 2009, **65**, 148–155.
- R. Pandey, R. K. Gupta, P.-Z. Li, Q. Xu, A. Misra and D. S. Pandey, *Org. Lett.*, 2012, **14**, 592–595.
- M. J. Hannon, S. Bunce, A. J. Clarke and N. W. Alcock, *Angew. Chem., Int. Ed.*, 1999, **38**, 1277–1278.
- F. Tuna, J. Hamblin, G. Clarkson, W. Errington, N. W. Alcock and M. J. Hannon, *Chem. – Eur. J.*, 2002, **8**, 4957–4964.
- H.-C. Wu, P. Thanasekaran, C.-H. Tsai, J.-Y. Wu, S.-M. Huang, Y.-S. Wen and K.-L. Lu, *Inorg. Chem.*, 2006, **45**, 295–303.
- B. Chakraborty, S. Maiti and T. K. Paine, *Polyhedron*, 2013, **52**, 122–127.
- G. C. van Stein, H. van der Poel, G. van Koten, A. L. Spek, A. J. M. Duisenberg and P. S. Pregosin, *J. Chem. Soc., Chem. Commun.*, 1980, 1016–1018.
- Y. Zhang, L. Xiang, Q. Wang, X.-F. Duan and G. Zi, *Inorg. Chim. Acta*, 2008, **361**, 1246–1254.
- P. K. Bowyer, K. A. Porter, A. D. Rae, A. C. Willis and S. B. Wild, *Chem. Commun.*, 1998, 1153–1154.
- M. J. Frisch, G. W. Trucks, H. B. Schlegel, G. E. Scuseria, M. A. Robb, J. R. Cheeseman, G. Scalmani, V. Barone, B. Mennucci, G. A. Petersson, H. Nakatsuji, M. Caricato, X. Li, H. P. Hratchian, A. F. Izmaylov, J. Bloino, G. Zheng, J. L. Sonnenberg, M. Hada, M. Ehara, K. Toyota, R. Fukuda, J. Hasegawa, M. Ishida, T. Nakajima, Y. Honda, O. Kitao, H. Nakai, T. Vreven, J. A. Montgomery, Jr., J. E. Peralta, F. Ogliaro, M. Bearpark, J. J. Heyd, E. Brothers, K. N. Kudin, V. N. Staroverov, R. Kobayashi,

- J. Normand, K. Raghavachari, A. Rendell, J. C. Burant, S. S. Iyengar, J. Tomasi, M. Cossi, N. Rega, J. M. Millam, M. Klene, J. E. Knox, J. B. Cross, V. Bakken, C. Adamo, J. Jaramillo, R. Gomperts, R. E. Stratmann, O. Yazyev, A. J. Austin, R. Cammi, C. Pomelli, J. W. Ochterski, R. L. Martin, K. Morokuma, V. G. Zakrzewski, G. A. Voth, P. Salvador, J. J. Dannenberg, S. Dapprich, A. D. Daniels, Ö. Farkas, J. B. Foresman, J. V. Ortiz, J. Cioslowski and D. J. Fox, *Gaussian 09, Revision D.01*, Gaussian, Inc., Wallingford CT, 2009.
- 47 J. P. Perdew, K. Burke and M. Ernzerhof, *Phys. Rev. Lett.*, 1996, **77**, 3865–3868.
- 48 J. P. Perdew, K. Burke and M. Ernzerhof, *Phys. Rev. Lett.*, 1997, **78**, 1396.
- 49 A. D. McLean and G. S. Chandler, *J. Chem. Phys.*, 1980, **72**, 5639–5648.
- 50 K. Raghavachari, J. S. Binkley, R. Seeger and J. A. Pople, *J. Chem. Phys.*, 1980, **72**, 650–654.
- 51 T. H. Dunning Jr. and P. J. Hay, *Modern Theoretical Chemistry*, ed. H. F. Schaefer III, Plenum, New York, 1976, vol. 3, pp. 1–28.
- 52 P. J. Hay and W. R. Wadt, *J. Chem. Phys.*, 1985, **82**, 270–283.
- 53 P. J. Hay and W. R. Wadt, *J. Chem. Phys.*, 1985, **82**, 299–310.
- 54 W. R. Wadt and P. J. Hay, *J. Chem. Phys.*, 1985, **82**, 284–298.
- 55 R. Dennington, T. Keith and J. Millam, *GaussView, Version 5*, Semichem Inc., Shawnee Mission KS, 2009.
- 56 Mercury CSD 2020, version 2.0, C. F. Macrae, I. J. Bruno, J. A. Chisholm, P. R. Edgington, P. McCabe, E. Pidcock, L. Rodriguez-Monge, R. Taylor, J. van de Streek and P. A. Wood, *J. Appl. Crystallogr.*, 2008, **41**, 466–470.